# SPATIALLY RESOLVED SPECTROPHOTOMETRY OF M81: AGE, METALLICITY, AND REDDENING MAPS

Xu Kong,[1,2] Xu Zhou,[1] Jiansheng Chen,[1] Fuzhen Cheng,[2,1] Zhaoji Jiang,[1] Jin Zhu,[1] Zhongyuan Zheng,[1] Shude Mao,[3,4] Zhaohui Shang,[1,5] Xiaohui Fan,[1,6] Yong-Ik Byun,[7,8] Rui Chen,[1] Wen-ping Chen,[7] Licai Deng,[1] Jeff J. Hester,[9] Yong Li,[9] Weipeng Lin,[1] Hongjun Su,[1] Wei-hsin Sun,[7] Wean-shun Tsay,[7] Rogier A. Windhorst,[9] Hong Wu,[1] Xiaoyang Xia,[10,1] Wen Xu,[1,9] Suijian Xue,[1] Haojing Yan,[1,9] Zheng Zheng,[1] and Zhenglong Zou[1]

## ABSTRACT

In this paper we present a multicolor photometric study of the nearby spiral galaxy M81, using images obtained with the Beijing Astronomical Observatory 60/90 cm Schmidt telescope in 13 intermediate-band filters from 3800 to 10000 Å. The observations cover the whole area of M81, with a total integration of 51 hr from 1995 to 1997 February. This provides a multicolor map of M81 in pixels of 1″.7 × 1″.7. Using theoretical stellar population synthesis models, we demonstrate that some BATC (Beijing-Arizona-Taiwan-Connecticut Multicolor Sky Survey) colors and color indices can be used to disentangle the age and metallicity effect. We compare in detail the observed properties of M81 with the predictions from population synthesis models and quantify the relative chemical abundance, age, and reddening distributions for different components of M81. We find that the metallicity of M81 is about $Z = 0.03$, with no significant difference over the whole galaxy. In contrast, an age gradient is found between stellar populations of the central regions and of the bulge and disk regions of M81: the stellar population in its central regions is older than 8 Gyr, while the disk stars are considerably younger ($\sim 2$ Gyr). We also give the reddening distribution in M81. Some dust lanes are found in the galaxy bulge region, and the reddening in the outer disk is higher than that in the central regions.

*Key words:* dust, extinction — galaxies: abundances — galaxies: evolution — galaxies: individual (M81) — galaxies: stellar content

## 1. INTRODUCTION

Spatially resolved information about the age, metallicity, and interstellar-medium reddening of galaxies is a powerful tool to study galaxy evolution, since it provides essential clues in star formation history, chemical composition, and enrichment history and environment of galaxies (Buzzoni 1989). To obtain such information, we need to know the stellar component and the overall properties of stellar populations (Leitherer & Heckman 1995). Ideally, one would like to study resolved individual stars in galaxies. However, given the limited spatial resolution of current telescopes, this is only possible for a few very nearby galaxies. As a result, the stellar content of even some relatively simple galaxies remains to be unraveled (Thuan 1991). Information of stellar population and star formation history in these galaxies, however, can still be obtained from studying the *integrated* properties of the stars (e.g., Schmitt, Bica, & Pastoriza 1996; Goerdt & Kollatschny 1998).

Since the pioneering work of Tinsley (1972) and Searle, Sargent, & Bagnuolo (1973), evolutionary population synthesis has become a standard technique to study the stellar populations of galaxies. This is a result of improvements in the theory of the chemical evolution of galaxies, star formation, stellar evolution and atmospheres and of the development of synthesis algorithms and the availability of various evolutionary synthesis models. A comprehensive compilation of such models was published by Leitherer et al. (1996) and Kennicutt (1998). Widely used models include those from the Padua and Geneva group (e.g., Schaerer & de Koter 1997; Schaerer & Vacca 1998; Bressan, Choisi, & Tantalo 1996; and Chiosi et al. 1998), GISSEL96 (Bruzual & Charlot 1991, 1993; GSSP[11]), PEGASE (Fioc & Rocca-Volmerange 1997) and STARBURST99 (Leitherer et al. 1999).

Many previous studies of integrated stellar populations use spectroscopic data, usually for limited regions in galaxies. In this paper we will instead use multicolor photometry to probe the stellar populations. The multicolor photometry provides accurate spectral energy distributions (SEDs) for the *whole* galaxy, although at low spectral resolution. We shall demonstrate that it is a powerful tool to study the structure and evolution of the galaxy, together with the theoretical evolutionary population synthesis methods (for an application of a similar technique, but with

---

[1] Beijing Astronomical Observatory and Beijing Astrophysics Center (BAC), National Astronomical Observational Center, Chinese Academy of Sciences, Beijing, 100012, China; xkong@mail.ustc.edu.cn.

[2] Center for Astrophysics, University of Science and Technology of China, Hefei, 230026, China.

[3] Max-Planck-Institut für Astrophysik, Karl-Schwarzschild-Strasse 1, 85740, Garching, Germany.

[4] University of Manchester, Jodrell Bank Observatory, Macclesfield, Cheshire SK11 9DL, UK.

[5] Department of Astronomy, University of Texas at Austin, Austin, TX 78712.

[6] Princeton University Observatory, Princeton, New Jersey, 08544.

[7] Institute of Astronomy, National Central University, Chung-Li, Taiwan.

[8] Center for Space Astrophysics and Department of Astronomy, Yonsei University, Seoul, 120-749, Korea.

[9] Department of Physics and Astronomy, Box 871504, Arizona State University, Tempe, AZ 85287-1504.

[10] Department of Physics, Tianjin Normal University, China.

---

[11] Galaxy Isochrone Synthesis Spectral Evolution Library available at: ftp://gemini.tuc.noao.edu/pub/charlot/bc96/.

fewer colors, to moderate redshifts, see Abraham et al. 1999). For this purpose, we pick M81 as the first application of this multicolor approach.

M81 is an excellent candidate because it is a nearby early-type Sab spiral galaxy at a distance of 3.6 Mpc and with an angular size of $\sim 26'$. The angular extent is large enough such that the disk and bulge regions are well separated from the ground. It has been the subject of numerous previous studies providing a wealth of information with which to compare the new metallicity and internal reddening distribution. The internal reddening has been studied by Kaufman et al. (1987, 1989), Devereux, Ford, & Jacoby (1997), Ho, Filippenko, & Sargent (1996), and Allen et al. (1997). The metallicity has been studied by Stauffer & Bothun (1984), Garnett & Shields (1987), Brodie & Huchra (1991), and Perelmuter, Brodie, & Huchra (1995). In this paper we present a further detailed study of M81 using the unique data set obtained from the Beijing-Arizona-Taiwan-Connecticut Multicolor Sky Survey (BATC).

The outline of the paper is as follows. Details of observations and data reduction are given in § 2. In § 3 we provide a brief description of the model and analyze the evolution of the integrated colors and color indices with age and metallicity. The observed two-dimensional SEDs of M81 were analyzed using stellar population synthesis models of GSSP. The distributions of metallicity, age, and interstellar reddening are given in § 4. In § 5 we discuss how different star formation histories and stellar population synthesis models change our results and compare our results with previous studies. The conclusions are summarized in § 6.

## 2. OBSERVATIONS AND DATA REDUCTION

### 2.1. *CCD Image Observation*

The large-field multicolor observations of the spiral galaxy M81 were obtained in the BATC photometric system. The telescope used is the 60/90 cm f/3 Schmidt telescope of Beijing Astronomical Observatory (BAO), located at the Xinglong station. A Ford Aerospace 2048 × 2048 CCD camera with 15 $\mu$m pixel size is mounted at the Schmidt focus of the telescope. The field of view of the CCD is $58' \times 58'$ with a pixel scale of $1''.7$.

The multicolor BATC filter system includes 15 intermediate-band filters, covering the total optical wavelength range from 3000 to 10000 Å (see Fan et al. 1996). The filters were specifically designed to avoid contamination from the brightest and most variable night sky emission lines. A full description of the BAO Schmidt telescope, CCD, data-taking system, and definition of the BATC filter systems is detailed elsewhere (Fan et al. 1996; Chen et al. 2000). To study the age, metallicity, and interstellar reddening of M81, the images of M81 covering most of the optical body of M81 were accumulated in 13 intermediate-band filters, with a total exposure time of about 51 hr from 1995 February 5 to 1997 February 19. The CCD images are centered at R.A. = $09^h55^m35^s.25$ and declination = $69°21'50''.9$ (J2000.0). The dome flat-field images were taken by using a diffuse plate in front of correcting plate of the Schmidt telescope. For flux calibration, the Oke-Gunn primary flux standard stars HD19445, HD84937, BD + 262606, and BD + 174708 were observed during photometric nights. The parameters of the filters and the statistics of the observations are given in Table 1.

### 2.2. *Image Data Reduction*

The data were reduced with standard procedures, including bias subtraction and flat-fielding of the CCD images, with an automatic data reduction software named PIPE-LINE 1 developed for the BATC multicolor sky survey (Fan et al. 1996). The flat-fielded images of each color were combined by integer pixel shifting. The cosmic rays and bad pixels were corrected by comparison of multiple images during combination. The images were recentered and position-calibrated using the *HST* Guide Star Catalog. The sky background of the images was obtained by fitting image areas free of stars and galaxies using the method described in Zheng et al. (1999). The absolute flux of intermediate-band filter images was calibrated using observations of standard stars. Fluxes as observed through the BATC filters

TABLE 1

PARAMETERS OF THE BATC FILTERS AND STATISTICS OF OBSERVATIONS

| No. (1) | Name (2) | cw[a] (Å) (3) | Exp. (hr) (4) | N.img[b] (5) | rms[c] (6) | Err.[d] (7) | SM.err.[e] (8) |
|---|---|---|---|---|---|---|---|
| 1....... | BATC02 | 3894 | 04:52 | 26 | 0.021 | 7.2 | 0.5 |
| 2....... | BATC04 | 4546 | 01:00 | 10 | 0.017 | 11.5 | 0.7 |
| 3....... | BATC05 | 4872 | 03:05 | 11 | 0.016 | 3.5 | 0.2 |
| 4....... | BATC06 | 5250 | 03:03 | 13 | 0.016 | 5.2 | 0.3 |
| 5....... | BATC07 | 5785 | 03:12 | 16 | 0.011 | 7.7 | 0.5 |
| 6....... | BATC08 | 6075 | 02:14 | 10 | 0.016 | 18.3 | 1.2 |
| 7....... | BATC09 | 6710 | 02:46 | 14 | 0.018 | 5.7 | 0.4 |
| 8....... | BATC10 | 7010 | 02:19 | 11 | 0.019 | 25.1 | 1.6 |
| 9....... | BATC11 | 7530 | 03:00 | 13 | 0.017 | 8.2 | 0.5 |
| 10...... | BATC12 | 8000 | 04:50 | 16 | 0.014 | 16.1 | 1.0 |
| 11...... | BATC13 | 8510 | 04:45 | 15 | 0.019 | 20.9 | 1.4 |
| 12...... | BATC14 | 9170 | 05:10 | 17 | 0.021 | 25.7 | 1.7 |
| 13...... | BATC15 | 9720 | 11:00 | 35 | 0.019 | 25.8 | 1.7 |

[a] Central wavelength for each BATC filter.
[b] Image numbers for each BATC filter.
[c] Zero-point error, in magnitude, for each filter as obtained from the standard stars.
[d] Background errors before image smoothing.
[e] Background errors after image smoothing.

TABLE 2

TWO DIMENSIONAL SPECTRAL ENERGY DISTRIBUTIONS FOR THE CENTRAL, BULGE, AND DISK AREAS OF M81

| | | FLUXES IN DIFFERENT FILTERS RELATIVE TO THE $F_{BATC08}$ FILTER | | | | | | | | | | | | |
|---|---|---|---|---|---|---|---|---|---|---|---|---|---|---|
| X (1) | Y (2) | 02 (3) | 04 (4) | 05 (5) | 06 (6) | 07 (7) | 09 (8) | 10 (9) | 11 (10) | 12 (12) | 13 (13) | 14 (14) | 15 (15) | FLUX OF BATC08 (16) |
| 4...... | 592 | 0.412 | 0.480 | 0.374 | 0.399 | 0.464 | 0.782 | 0.532 | 0.610 | 0.888 | 0.870 | 1.059 | 0.843 | 29.0 |
| 4...... | 593 | 0.391 | 0.460 | 0.354 | 0.374 | 0.456 | 0.770 | 0.519 | 0.606 | 0.903 | 0.859 | 1.067 | 0.845 | 31.0 |
| 5...... | 277 | 0.204 | 0.420 | 0.558 | 0.714 | 0.844 | 0.846 | 1.013 | 1.400 | 1.309 | 1.484 | 1.737 | 1.635 | 63.0 |
| 5...... | 278 | 0.180 | 0.382 | 0.480 | 0.615 | 0.785 | 0.841 | 0.966 | 1.423 | 1.279 | 1.409 | 1.732 | 1.536 | 74.0 |
| 5...... | 279 | 0.201 | 0.392 | 0.537 | 0.687 | 0.827 | 0.811 | 0.962 | 1.425 | 1.268 | 1.435 | 1.670 | 1.540 | 66.0 |

NOTE.—Table 2 is presented in its entirety in the electronic edition of the Astronomical Journal. A portion is shown here for guidance regarding its form and content.

for the Oke-Gunn stars were derived by convolving the SEDs of these stars with the measured BATC filter transmission functions (Fan et al. 1996). Column (6) in Table 1 gives the zero-point error, in magnitude, for the standard stars in each filter. The formal errors we obtain for these stars in the 13 BATC filters is $\lesssim 0.02$ mag. This indicates that we can define the standard BATC system to an accuracy of $\lesssim 0.02$ mag.

After background subtraction, the standard deviation of the background for each image is 2.0 ADU. Because the signal-to-noise ratio (S/N) decreases from the center to the edge of the galaxy, we smoothed the images with a boxcar filter. The window sizes of the boxcar were selected depending on the ADU values of the BATC10 band image (7010 Å). If the ADU value was less than 100, the pixel was set to zero; if the value was higher than 100, the pixel was adaptive-smoothed by boxcar filter of $N \times N$ (cell size), where $N = \min [151 (ADU_{BATC10})^{-1}, 15]$. By this method, the images were smoothed depending on the S/N of each cell. In the central area of M81, the original pixels were used, whereas near the edge of M81 the mean value of multiple pixels (cells) were used; as a result, the spatial resolution decreased from center to outer edge. The background errors before and after smoothing are given in the last two columns in Table 1.

Finally, the flux derived at each point of M81 is listed in Table 2. The results provide a two-dimensional spectral energy distribution (SED) for M81. The ADU number of each image was converted into units of $10^{-30}$ ergs s$^{-1}$ cm$^{-2}$ Hz$^{-1}$. As an example, we present some SEDs for the different areas of M81 in this paper. The table gives the following information: columns (1) and (2) give the $(X, Y)$ positions of the photometric center of the regions, in units of arcseconds. The coordinate system is centered on the nucleus of the galaxy (R.A. = $09^h55^m35\overset{s}{.}25$; decl. = $69°21'50\overset{''}{.}9$, in J2000.0). The x-axis is along the east-west direction with positive values toward the east, and the y-axis is along the north-south direction with positive values toward the north. Columns (3)–(14) give the fluxes relative to the BATC08 filter (6075 Å). Column (15) gives the flux in the BATC08 filter in units of $10^{-30}$ ergs$^{-1}$ cm$^{-2}$ Hz$^{-1}$. For convenience in later discussions, we define the "central" areas as regions with $|\Delta R.A.| \leq 1\overset{'}{.}0, |\Delta DEC| \leq 1\overset{'}{.}9$, the "bulge" region with $1.0 < |\Delta RA| \leq 3\overset{'}{.}4, 1\overset{'}{.}9 < |\Delta DEC| \leq 4\overset{'}{.}0$ and the "disk" region with $3\overset{'}{.}4 < |\Delta RA| \leq 6\overset{'}{.}2, 4\overset{'}{.}0 < |\Delta DEC| < 8\overset{'}{.}0$.

We show a black and white image of M81 in Figure 1.[12] The filters selected here are free from any strong emission lines. From this image, we can see directly the stellar population difference in different areas of the spiral galaxy M81. In the following sections we will analyze quantitatively the stellar populations in M81 with our 13 color data.

The bright H II regions consist of young clusters, and the evolutionary population synthesis methods used in this paper do not represent young clusters well. In addition, the central nucleus of M81 exhibits some of the same characteristics as classical Seyfert galaxies; it has no evidence of stellar clusters or a population of hot young stars (Kaufman et al. 1996; Devereux et al. 1997; Davidge & Courteau 1999). So we mask some bright H II regions and the central nucleus of M81 (shown as white spots in Figs. 4a, 5, and 6, including the foreground stars) in this paper.

### 3. DATABASES OF SIMPLE STELLAR POPULATIONS

A simple stellar population (SSP) is defined as a single generation of coeval stars with fixed parameters such as metallicity, initial mass function, etc. (Buzzoni 1997). In evolution synthesis models, they are modeled by a collection of stellar evolutionary tracks with different masses and initial chemical compositions, supplemented with a library of stellar spectra for stars at different evolutionary stages because SSPs are the basic building blocks of synthetic spectra of galaxies that can be used to infer the formation and subsequent evolution of the parent galaxies (Jablonka et al. 1996). In order to study the integrated properties of the stellar population in M81, as a first step, we use the SSPs of the GSSP. We study the SSPs as the first step for two reasons. First, they are simple and reasonably well understood, so it is important to see what one can learn using this simplest assumption and then check whether more complex star formation history give qualitatively similar conclusions. This is a common approach often taken in the evolutionary population synthesis models for galaxies (Vazdekis et al. 1997; Mayya 1995). Second, although we assume each pixel is described by an SSP, we emphasize that the whole galaxy is not SSP; so our assumption is not as strong as it may seem. Nevertheless, this is a significant

---

[12] To display the features more clearly, a "true-color" image of M81 is presented in the electronic edition of the Astronomical Journal.

FIG. 1.—Estimate of M81 generated by using the BATC02 (3894 Å) filter image for blue, BATC07 (5785 Å) for green, and BATC10 (7010 Å) for red; the image is balanced by making the background old population orange and hot stars blue. The center (origin) of the image is located at $\alpha = 09^h55^m35\overset{s}{.}25$, $\delta = 69°21'50\overset{''}{.}9$ (J2000.0). The image size is about $17\overset{'}{.}0$ by $21\overset{'}{.}0$. North is up, and east to the left. We refer to the region with $|\Delta RA| \leq 1\overset{'}{.}0, |\Delta DEC| \leq 1\overset{'}{.}9$ as the central region, the region with $1.0 < |\Delta RA| \leq 3\overset{''}{.}4, 1.9 < |\Delta DEC| \leq 4\overset{''}{.}0$ as the bulge, and the region with $3\overset{'}{.}4 < |\Delta RA| \leq 6\overset{'}{.}2, 4\overset{'}{.}0 < |\Delta DEC| < 8\overset{'}{.}0$ as the disk. A "true-color" image of this figure is available in the electronic edition of the Astronomical Journal.

$C_{3894}$

$C_{4546}$

$C_{4872}$

$C_{5250}$

Z=0.10
Z=0.05
Z=0.02
Z=0.008
Z=0.004
Z=0.0004

KONG ET AL.
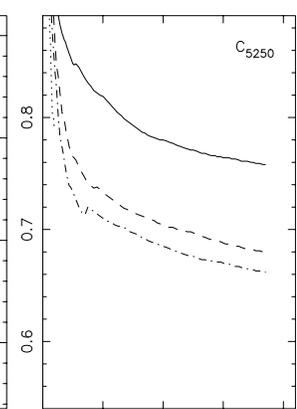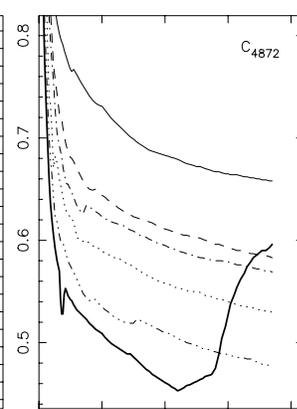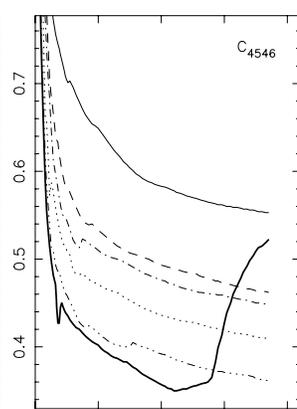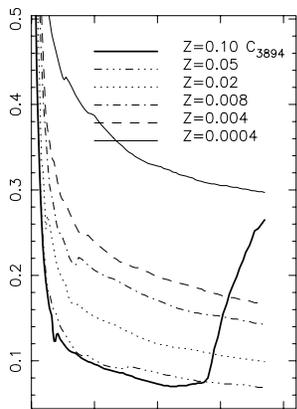
SSPs to become redder for all colors as the metallicity increases from $Z = 0.0004$ to $Z = 0.05$. The near-UV and optical colors show the same qualitative behavior as those at longer wavelengths. (2) There is a wide range in age (from 1 to 20 Gyr) in which the colors vary monotonically with time except for the highest metallicity $Z = 0.1$. Therefore, once we know the metallicity and interstellar reddening, we can use these colors to determine the age distribution of M81, provided that the stellar population is well modeled by SSPs. (3) For $Z = 0.1$, there is only a limited age range for the monotonic behavior in colors. One reason for this behavior is the appearance of AGB-manqué stars at $Z = 0.1$. These stars skip the AGB phase and directly go through a long-lived hot HB phase (GSSP). There are very few, if any, examples of galactic stars with such a high metallicity. So our results are not affected by this peculiar high-metallicity case.

### 3.3. Color Indices of GSSPs

The observed colors are affected by interstellar reddening, which will of course complicate our interpretations (Östlin, Bergvall, & Bönnback 1998). The interstellar reddening in the center region of M81 can be measured by its emission lines, but for the outer regions, the problem becomes very complex. If we suppose that the extinction law from 3800 to 10000 Å has no high-frequency features, the spectral indices will not be affected much by the uncertainties in the extinction, so we can use the spectral indices to reduce the effect of interstellar extinction.

Spectral indices are (by definition) constructed by means of a central bandpass and two pseudo-continuum bandpass on either side of the central band. The continuum flux is interpolated between the middle points of the pseudo-continuum bandpasses (Bressan et al. 1996; Worthey & Ottaviani 1997). Since we only observed M81 with intermediate-band filters, not a genuine one-dimensional spectrum, we must use some pseudo-color indices to replace the conventional definitions. We define a color index

$I_{\lambda_j}(t, Z)$ of a SSP by

$$ I_{\lambda_j}(t, Z) = L_{\lambda_j}(t, Z)/L_{\lambda_{j+1}}(t, Z) , \qquad (3) $$

where $L_{\lambda_j}(t, Z)$ is the luminosity of a SSP with the metallicity $Z$ at age $t$ and wavelength $\lambda_j$, $L_{\lambda_{j+1}}(t, Z)$ is the luminosity in the $(j + 1)$th filter for the same SSP. The color indices can reduce the effect of reddening, especially in the wavelength region longer than 5000 Å.

Among all the BATC filter bands, we find that the color index centered at 8510 Å ($I_{8510}$) is much more sensitive to the metallicity than to the age; the center of this filter band is near the Ca II triplets ($\lambda\lambda = 8498, 8542, 8662$ Å). The strength of Ca II triplet depends on the effective temperature, surface gravity, and the metallicity for late-type stars (Zhou 1991).

In an old stellar system, the effect of metallicity on Ca II triplet becomes prominent. In fact, we find that there is a very good relation between the flux ratio of $I_{8510} \equiv L_{8510}/L_{9170}$ and the metallicity for stellar populations older than 1 Gyr. We plot this relation in Figure 3. Similar relations are also found in many other observation and stellar population synthesis models.

The relation shown in Figure 3 is crucial for our metallicity determination and later studies, so it is important to check whether this is indeed a reliable method. An early study by Alloin & Bica (1989), based on the analysis of stars, star clusters, and galaxy nuclei indicated a strong correlation of Ca II triplet with the surface gravity, $\log g$. However, further studies suggested that the Ca II triplet strength depends not only on the surface gravity but also on the metallicity. A detailed analysis of the behavior of the Ca II triplet feature as a function of stellar parameters was performed by Erdelyi-Mendes & Barbuy (1991), making use of a large grid of synthetic spectra. They concluded that Ca II triplet has a weak dependence on the effective temperature, a modest dependence on surface gravity, but a quite important dependence on metallicity. They even suggested that the Ca II triplet strength may vary exponentially
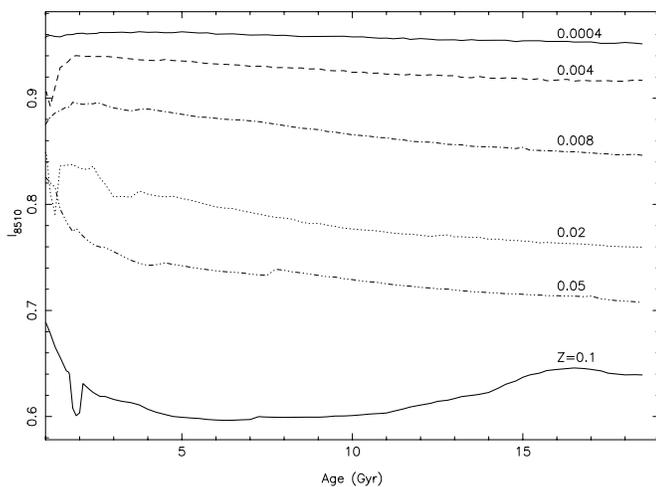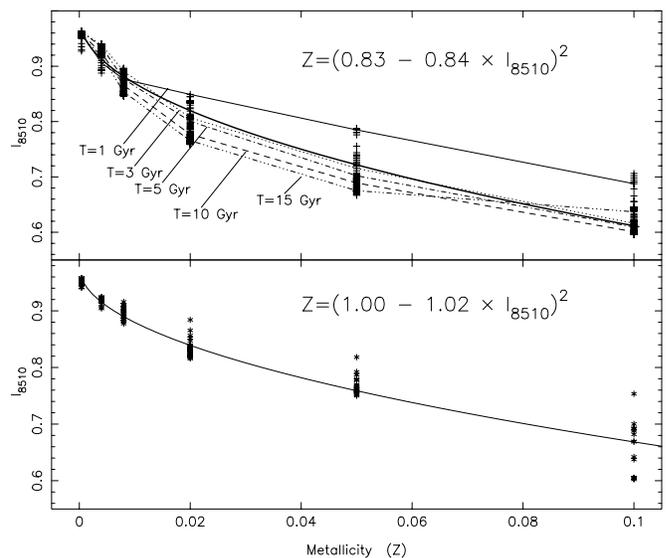


Fig. 3a



Fig. 3b

FIG. 3.—(a) Dependence of the pseudo-color index $I_{8510}$ with metallicity for the GISSEL96 SSP models. The line symbols are the same as in Fig. 2. The metallicities are labeled above each line. (b) Correlation between the pseudo-color index $I_{8510}$ and metallicity, for five different ages ($T = 15, 10, 5, 3, 1$ Gyr). The solid line shows the best fit through the curves. The bottom panel is for the PSSPs, the top panel for the GSSPs.
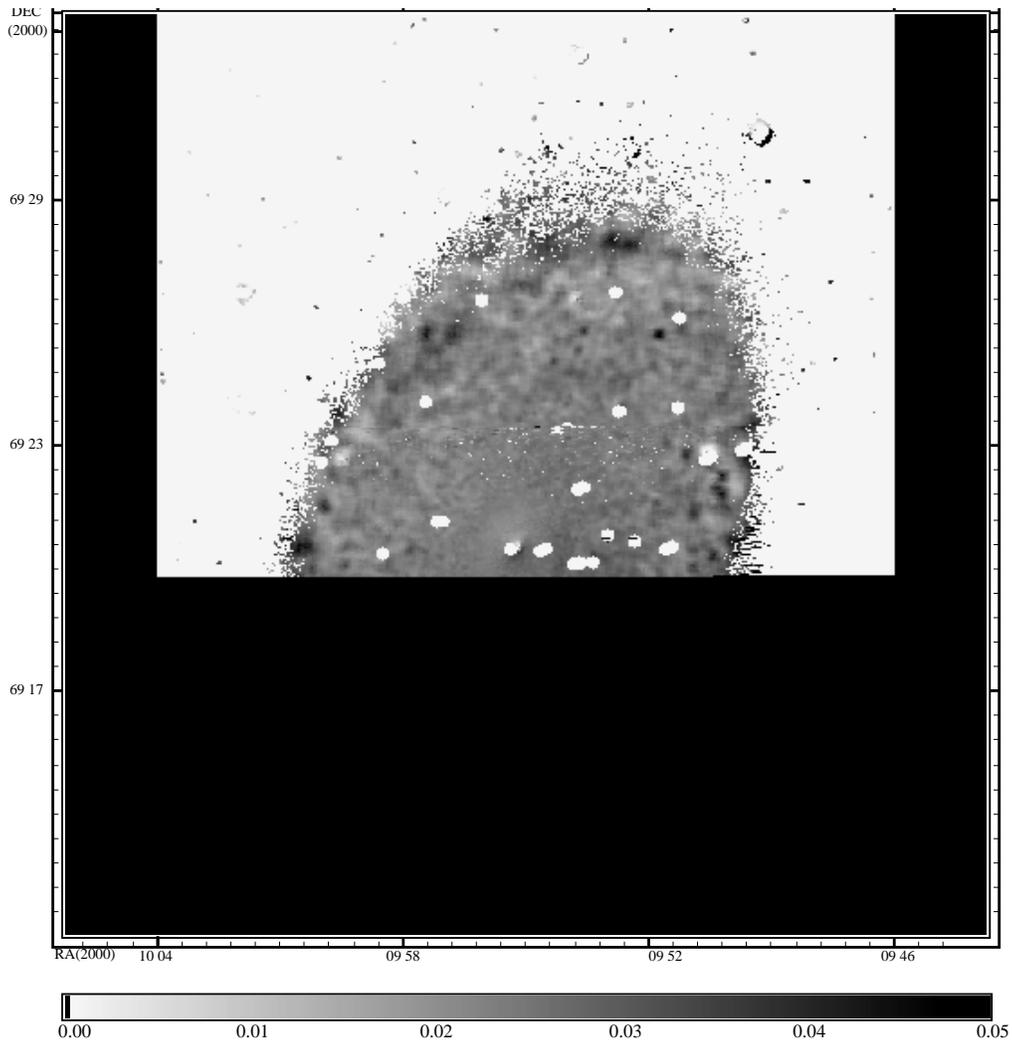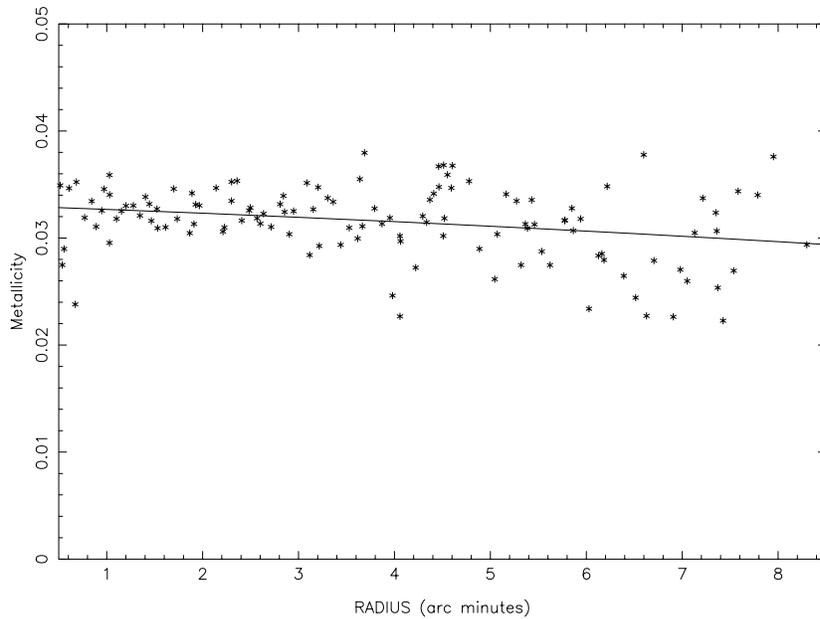
FIG. 4a



FIG. 4b

FIG. 4.—(a) Map of the population metallicity in M81. Light gray corresponds to low, and dark gray to high metallicity. Some bright H II regions, the central nucleus of M81, and most of foreground stars are masked, shown as white spots. (b) Radial distribution of metallicity for M81, averaging over ellipses along the major axis (its position angle is taken to be 157°). The line is the regression line obtained by a polynomial fit. No obvious metallicity gradient exists from the central region to the bulge and disk of M81.
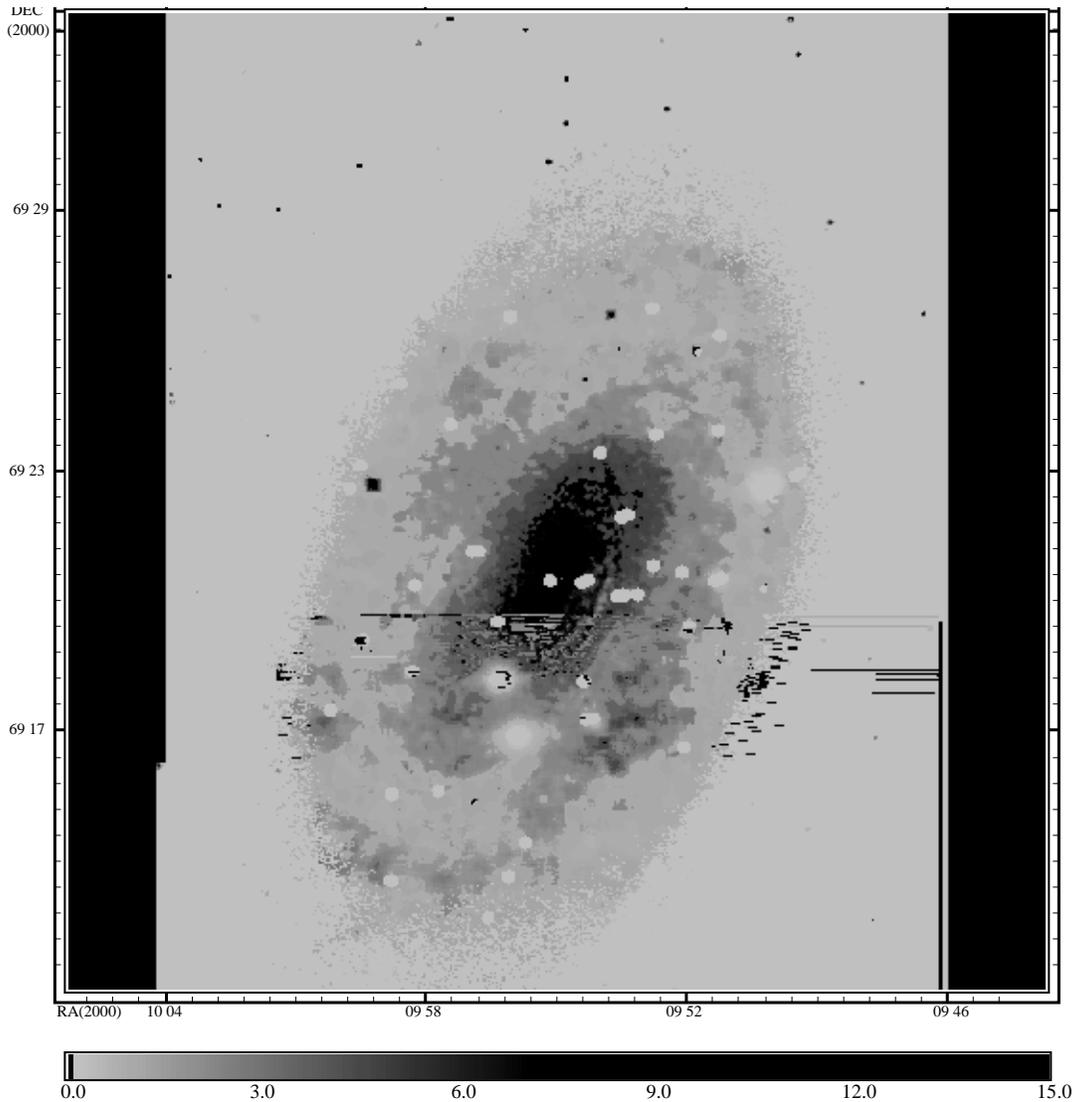
FIG. 5.—Map of the population ages in M81. Light gray corresponds to the young and dark gray to the oldest zones. As in Fig. 4a, the white spots represent the masked regions, such as bright H II regions, the central nucleus of M81, and most of foreground stars.

with the metallicity. Moreover, these lines have been studied by Diaz, Terlevich, & Terlevich (1989), Mallik (1994), and Idiart, Thévenin, & de Freitas Pacheco (1997). They have also suggested the Ca II triplet strengths depend on the metallicity (Mayya 1997). So the relation between the $I_{8510}$ and metallicity seems to be reliable and can be used to determine the metallicities; our own investigation of GSSPs seems to be consistent with these recent studies.

## 4. DISTRIBUTION OF METALLICITY, AGE, AND REDDENING

In general, the SED of a stellar system depends on age, metallicity, and reddening along the line of sight. The effects of age, metallicity, and reddening are difficult to separate (e.g., Calzetti 1997; Origlia et al. 1999, Vazdekis et al. 1997). Older age, higher metallicity, or larger reddening all lead to a redder SEDs of stellar systems in the optical (Mollà, Ferrini, & Diaz 1997; Bressan et al. 1996). In order to separate the effects of age, metallicity, and interstellar reddening of M81, we first determine the metallicity by the color index $I_{8510}$, as discussed above, and then obtain the

age and reddening by using GSSP model of known metallicity and a extinction law (see § 4.2).

### 4.1. Metallicity Distribution

As discussed in § 3.3, there is a good correlation between the color index $I_{8510}$ and the metallicity. We will use the relation obtained from GSSP; this relation is similar for other stellar population synthesis models. We find that the correlation can be fitted with a simple formula,

$$Z = (0.83 - 0.84 \times I_{8510})^2 . \qquad (4)$$

This curve is shown in the top panel of Figure 3. The scatter in Figure 3 is due to the difference in age. If the ages are younger than 1 Gyr, the scatter becomes larger. Figure 3 shows that for a stellar system of ages older than 0.5 Gyr, we can estimate the metallicity with an error less than the interval of metallicity given by GSSP.

Using this method we obtained the metallicities for each part of M81 except for the nucleus and the Hα line emission region (we have masked them out, see § 2.2). Figure 4a shows the resulting metallicity map of M81. Figure 4b shows the radial distribution of the metallicity; the curve is
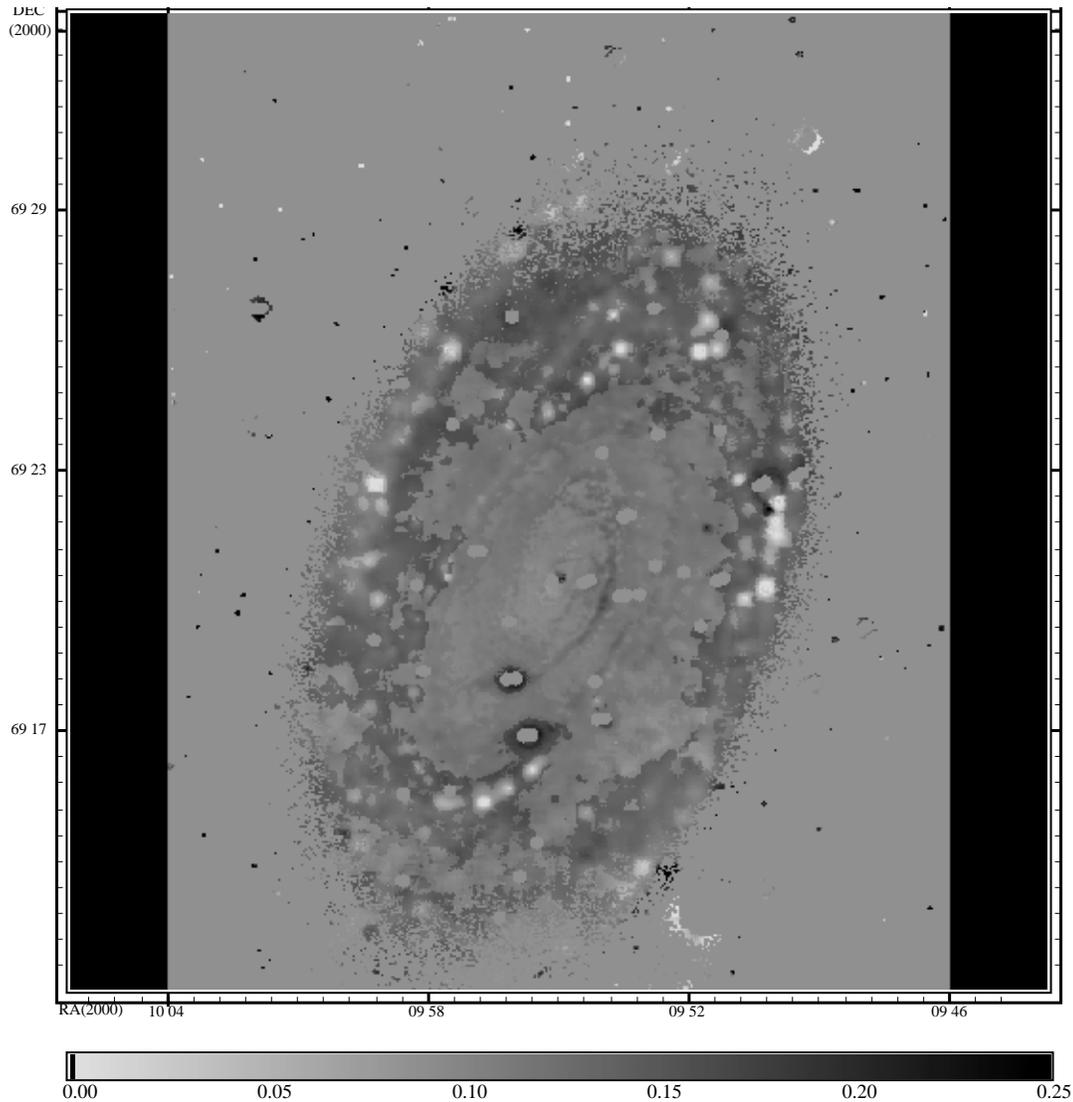
FIG. 6.—Interstellar reddening map of M81, using the method described in the text

derived from the Fig. 4a by averaging over ellipses of widths 17″ along the major axis. We used an inclination angle of $i = 59°$ and a position angle of P.A. = 157° for the major axis of the galaxy.

To our surprise, we do not find, within our errors, any obvious metallicity gradient from the central region to the bulge and disk of M81. In most parts of M81, the mean metallicity is about 0.03, with variation $\lesssim 0.005$. These results are identical to past suggestions that early-type spirals may have relative high abundances and weak gradients. Taking into account the age scatter, the true value of the metallicity is likely within a range between $Z = 0.02$ and $Z = 0.05$. From the metallicity map of M81, we can also clearly see that in some outer regions the metallicities are higher; most of these regions are located in spiral arms and around H II regions, where a younger stellar population is present.

### 4.2. Age and Reddening Distribution

Since we model the stellar populations by SSPs, the observed colors for each cell are determined by two parameters: age, $t$, and dust reddening, $E(B-V)$. In this section,

we will determine these parameters for M81 simultaneously by a least-squares method. The procedure is as follows. For given reddening and age (recall that the metallicity is known; see previous subsection), we can obtain the predicted integrated colors by convolving the dust-free predictions from GSSP with the extinction curve given by Zombeck (1990). The best-fit age and reddening values are found by minimizing the difference between the observed colors and the predicted values:

$$R^2(x, y, t, Z, E) = \sum_{i=1}^{12} [C_{\lambda_i}^{obs}(x, y) - C_{\lambda_i}^{ssp}(t, Z, E)]^2 , \quad (5)$$

where $C_{\lambda_i}^{ssp}(t, Z, E)$ represents integrated color in the $i$th filter of a SSP with age $t$, metallicity $Z$, and reddening correction $E$, and $C_{\lambda_i}^{obs}(x, y)$ is the observed integrated color at position $(x, y)$.

Figure 5 shows the age map for M81. It clearly indicates that the stellar population in the central regions is much older than that in the outer regions and that the youngest components reside in the spiral arms of M81. There is a smooth age gradient from the center of the galaxy to the edge of the bulge. The age in the innermost central region (within 17″) is older than $\gtrsim 15$ Gyr. The age at the more

extended central region is about 9 Gyr. In the bulge edge area, the age is about 4 Gyr. In contrast, the stellar component in the disk area is much younger than that in the bulge region. The mean age in disk area is about 2 Gyr. We can see that the age in spiral arms is even younger than the inter-arm areas, about 1 Gyr.

Because the age obtained in the outer disk region is around 1 Gyr, the metallicity, which is determined by the color indices, might have large errors (see § 4.1). The errors in turn will make the age determination uncertain. Therefore, the age for disk can only be regarded as a rough estimation. However, the general trend in the age distribution should be reliable.

Figure 6 shows the reddening map for M81. From this figure, we find a large difference in reddening between the bulge and the disk. In the bulge, the reddening, $E(B-V)$, is in the range of 0.08 to 0.15. For regions where $E(B-V)$ is larger than 0.1, we found some spiral-like cirrus. There is a very obvious high-reddening lane around the nucleus with reddening equal to or higher than the disk area. The maximum of $E(B-V)$ in the lane reaches 0.25. This half-loop lane can be verified in the future with IR or CO line observations. In the disk area, the mean reddening of $E(B-V)$ is about 0.2. In the central regions, the mean reddening of $E(B-V)$ is very small. These results suggest that dust is largely absent in the central regions of M81. The dust seems to be distributed mainly along the inner part of spiral arms and around the nucleus.[13]

## 5. DISCUSSION

The results we presented so far are based on the (strong) assumption that all stars in a small region form in an instantaneous burst, and hence the stellar population of each cell can be modeled as SSPs. Unfortunately, the star formation rate history is an essential but very uncertain ingredient in the evolutionary population synthesis method, since it can vary from galaxy to galaxy and from region to region inside a single galaxy as well. It is only for simplicity that we have adopted an instantaneous star formation history; clearly it is important to check whether the results are significantly changed if one varies the star formation history. We address this issue in § 5.1. While there seems to be general agreement between the GISSEL96 SSPs models (which we used) with other similar ones (Charlot, Worthey, & Brissan 1996), there are some fine differences. In § 5.2 we study how the results are changed if we adopt a different population synthesis model from the Padua group. In § 5.3 we compare our results with earlier works.

### 5.1. *Continuous Star Formation*

We assume that stars are formed from the interstellar gas exponentially with a characteristic timescale, $\tau$; i.e., $\Psi(t) = \Psi_0 \exp^{-t/\tau}$. This model is often used to calculate the integrated colors of galaxies (Kennicutt 1998) and allows a more diverse star formation history. If $\tau \to \infty$ the model approximates constant star formation rate, while for $\tau \to 0$ it approximates an instantaneous burst (Abraham et al. 1999). It seems that spiral galaxies could be well fitted with $\tau$ of the order of several gigayears (Fioc & Rocca-Volmerange 1997).

---

[13] Color versions of Figures 4–6 are available in the electronic edition of the Astronomical Journal.

Since we do not know the appropriate $\tau$ value for M81, we have explored the values $\tau = 0.1, 1, 3$ Gyr. We have calculated the age, metallicity, and interstellar reddening distributions for each value of $\tau$. As the value of $\tau$ increases, the age ($t$) increases throughout M81, while the interstellar reddening decreases and the metallicity is little changed. Although the numerical values of these quantities do change in each point of M81, the two-dimensional distributions of age, metallicity, and interstellar reddening of M81 for different values of $\tau$ are similar to the ones shown in Figures 4–6.

### 5.2. *Comparison with Other SSP Models*

There exist a number of SSP models that are synthesized with different approaches. It is important to check the sensitivity of our results to the SSP models adopted. The SSP models from the Padua group (hereafter, PSSPs) are suitable for the comparison, because they use a similar technique of "isochrone synthesis" to predict the spectral evolution of stellar populations. The PSSPs provide the basis for the population synthesis models (Bressan, Chiosi, & Fagotto 1994; see also Bressan et al. 1996 for revisions and extensions). The PSSPs use a comprehensive set of stellar evolutionary tracks of the Padua group for a wide range of initial chemical compositions from $Z = 0.0004$ to $Z = 0.1$ with $\Delta Y/\Delta Z = 2.5$. The initial masses of the evolutionary tracks cover the range of $0.6$–$120\ M_\odot$, except for the set of metallicity $Z = 0.1$, where the masses are from $0.6$–$9$ $M_\odot$. The initial mass function is the Salpeter (1955) law. More details can be found in Bressan et al. (1994), Silva (1995), and Tantalo et al. (1996). The main difference between GSSPs and PSSPs is the library of stellar spectra: the GSSPs use theoretical stellar spectra from Lejeune et al. (1997), while the PSSPs use theoretical stellar spectra from Kurucz (1992).

Using our method, we calculate the colors and color indices for each PSSP in the BATC filter system. Using similar procedures as for the GSSP (see § 4), we obtained the metallicity, age, and reddening distributions of M81. For PSSP, the metallicity map of M81 again has no obvious metallicity gradient, but the mean metallicity is somewhat higher, about 0.035. There is a smooth age gradient from the center of M81 to the edge of the bulge, except that the mean age in the disk area is lower than 1 Gyr. The interstellar reddening value from PSSP is obvious bigger than that from GSSP. In the bulge, the reddening value is in the range of 0.18 to 0.35. In the disk area, the mean reddening of $E(B-V)$ is about 0.40. The reddening value in the central region amounts to 0.15. The distributions of metallicity, age, and interstellar reddening are very similar to those found using GSSP.

### 5.3. *Comparison with Previous Work*

Numerous determinations of the amount of extinction in M81 have recently been obtained. Allen et al. (1997) compared the detailed distribution of H I, H$\alpha$, and 150 nm far-UV continuum emission in the spiral arms of M81. They found every reliable bright peak in the H$\alpha$ has a peak in the far-UV and concluded that the effects of extinction on the morphology are small on the spiral arms. Filippenko & Sargent (1988), based on the ratio of the narrow components of H$\alpha$ and H$\beta$, concluded that the central regions of M81 is reddened by $E(B-V) = 0.094$ mag. These results are

very similar to our results for internal reddening, that the mean reddening in the spiral arms and in the central regions of M81 is small. In addition, Kaufman et al. (1987, 1989), using the Hα and radio continuum (Bash & Kaufman 1986) observations, have studied the distribution of extinction along the spiral arms in M81 and obtained a mean $A_v = 1.1 \pm 0.4$ mag for 42 giant H II regions with high surface brightness. Hill et al. (1992) used near-UV, far-UV, and $V$-band images of M81 and cluster models to derive $A_v = 1.5$ mag for the H II regions on the arms. These internal reddening values are larger than ours for spiral arms. The discrepancy can be explained with reference to two reasons. First, the internal reddening value of Kaufman et al. is derived from the giant H II regions of M81 with high surface brightness, while these bright H II regions are excluded from our study. So we have used different regions for the internal reddening study, and it is therefore not clear that they must agree. Second, the continuum regions are affected less by reddening than the emission-line regions in a galaxy. The internal reddening value of Kaufman et al. is the reddening for emission-line regions, while our results are from the continuum regions. The former is significantly larger than the latter; this systematic difference has been seen in many other emission-line galaxies (Kong & Cheng 1999; Calzetti 1997).

Perelmuter et al. (1995) have obtained spectra for 25 globular clusters in M81. Following the method of Brodie & Huchra (1990), based on the weighted mean of six indices, they measured these clusters' metallicity. The mean metallicity was calculated both from the weighted mean of the individual metallicities and directly from the cumulative spectrum of the 25 globulars. Both results yielded the same value, $\langle Fe/H \rangle = -1.48 \pm 0.19$ ($Z = 0.033$), which is identical to that derived by Brodie & Huchra (1991) using eight clusters ($\langle Fe/H \rangle = -1.46 \pm 0.31$). No correlation has been observed between magnitude and metallicity of the globulars in the Milky Way and in M31. Thus the mean metallicity of the 25 globulars should be representative of the M81 system as a whole. These results agree with our results for the metallicity of M81 ($Z \approx 0.03$) very well. On the other hand, using the low-dispersion spectra of 10 H II regions in M81, Stauffer & Bothun (1984) estimated the oxygen abundances for those H II regions from the observed emission lines. They derived a mean abundance near solar and a weak abundance gradient in M81. Using the empirical calibration method and the photoionization models, Garnett & Shields (1987) have analyzed the metallicity abundance and abundance gradients for 18 H II regions in the galaxy M81. The major result of this study is the presence of an order-of-magnitude gradient in the oxygen abundance across the disk of M81. These results differ from ours. However, the differences can be readily explained. First, as for the internal reddening, the previous results are derived from the bright H II regions of M81; the abundance gradient is therefore for these H II regions. But our result comes from the whole galaxy *except* these bright H II regions. So it is not clear that they should have the same behaviors in metallicity. Another caveat to the previous results is that the Pagel, Edmunds, & Smith (1980) abundance calibration (which was used in Stauffer & Bothun 1984; Garnett & Shields 1987) is not expected to be exact.

Finally, we must emphasize that although the method we used in this paper can be used to constrain the variation of metallicity, population age, and reddening across M81 for the central region, the bulge, and the disk minus the spiral arms, it may not be suited to study the property of the spiral arms. There are two main reasons. First, there are hundreds of H II regions on the spiral arms, and the evolutionary population synthesis methods we used in this paper are not well represented very young clusters. Second, the signal-to-noise ratio decreases from the center to the edge of the galaxy; we have smoothed the images with a boxcar filter (see § 2.2). For the outer disk regions, such as the spiral arms, the smoothing tends to blend the hundreds of H II regions with their surroundings. We will study these bright H II regions at the spiral arms of M81 in more detail in a subsequent paper when we have better data, using the evolutionary population synthesis method, and show how well it can work for young clusters.

## 6. CONCLUSIONS

In this paper, we have, for the first time, obtained a two-dimensional SED of M81 in 13 intermediate colors with the BAO 60/90 cm Schmidt telescope. Below, we summarize our main conclusions.

1. Using the new extensive grid of GSSPs covering a wide range of metallicity and age, we calculated the colors and color indices for 13 colors in BATC intermediate-band filter system. We find that some of them can be used to break the age and metallicity degeneracy, which enables us to obtain two-dimensional maps of metallicity, interstellar reddening and age of M81.

2. From the two-dimensional metallicity distribution of M81, we find no obvious metallicity gradient from the central regions to the outer disk. In most of M81, the mean metallicity is about 0.03, with a variation $\lesssim 0.005$. Some regions in M81, however, have higher metallicity; they are mostly located in the spiral arms and around H II regions, where the younger component resides.

3. From the two-dimensional age distribution in M81, we find that the mean ages of the stellar populations in the central regions are older than those in the outer regions, which suggests that star formations in the central regions occurred earlier than the outer regions.

4. We find a strong difference in reddening between the bulge region and the disk region. In the bulge area, the reddening, $E(B-V)$, is in the range of 0.08 to 0.15. The mean reddening in the disk area is higher, about 0.2. There are some high-reddening spiral-like cirrus in the bulge.

5. In order to understand how sensitive our method is to different assumptions about star formation history and different stellar population synthesis models, we have studied an exponential star formation history and compared the results obtained with GSSP and PSSP. We find that, although the precise values of age, metallicity, and interstellar reddening are different, the general trend of in the metallicity, age, and reddening distributions is similar.

6. Finally, we have compared the internal reddening and metallicity maps of M81 with previous studies. We find that the agreements are generally good. In addition, we find that the properties for the bright H II regions and other parts may be different.

The results of M81 presented here illustrate that our method and observational data provide an efficient way to study the distribution of metallicity, age, and interstellar reddening for nearby face-on galaxies. Similar data have

already been collected for the similar galaxies M31, NGC5589, and NGC5055. The analysis results of these galaxies will be published in a forthcoming paper.

## REFERENCES

Abraham, R. G., Ellis, R. S., Fabian, A. C., Tanvir, N. R., & Glazebrook, K. 1999, MNRAS, 303, 641
Allard, F., & Hauschildt, P. H. 1995, ApJ, 445, 433
Allen, R. J., Knapen, J. H., Bohlin, R., & Stecher, T. P. 1997, ApJ, 487, 171
Alloin, D., & Bica, E. 1989, A&A, 217, 57
Bash, F. N., & Kaufman, M. 1986, ApJ, 310, 621
Bessell, M. S., Brett, J. M., Scholz, M., & Wood, P. R. 1991, A&AS, 89, 335
Bressan, A., Chiosi, C., & Fagotto, F. 1994, ApJS, 94, 63
Bressan, A., Chiosi, C., & Tantalo, R. 1996, A&A, 311, 425
Bressan, A., Fagotto, F., Bertelli, G., & Chiosi, C. 1993, A&AS, 100, 647
Brodie, J.P., & Huchra, J. P. 1990, ApJ, 362, 503
———. 1991, ApJ, 379, 157
Bruzual, G., & Charlot, S. 1993, ApJ, 405, 538
Buzzoni, A. 1989, ApJS, 71, 817
———. 1997, in IAU Symp. 183, Cosmological Parameters and the Evolution of the Universe, ed. K. Sato (Boston: Kluwer), 18
Calzetti, D. 1997, AJ, 113, 162
Charlot, S., & Bruzual, G. 1991, ApJ, 367, 126
Charlot, S., Worthey, G., & Bressan, A. 1996, ApJ, 457, 625
Chen, J.-S., et al. 2000, in preparation
Chiosi, C., Bressan, A., Portinari, L., & Tantalo, R. 1998, A&A, 339, 355
Davidge, T. J., & Courteau, S. 1999, AJ, 117, 2781
Devereux, N. A., Ford, H., & Jacoby, G. 1997, ApJ, 481, L71
Diaz, A., Terlevich, E., & Terlevich, R. 1989, MNRAS, 239, 325
Erdelyi-Mendes, M., & Barbuy, B. 1991, A&A, 241, 176
Fagotto, F., Bressan, A., Bertelli, G., & Chiosi, C. 1994, A&AS, 105, 39
Fan, X.-H., et al. 1996, AJ, 112, 628
Fioc, M., & Rocca-Volmerange, B. 1997, A&A, 326, 950
Filippenko, A. V., & Sargent, W. L. W. 1988, ApJ, 324, 134
Fluks, M. A., Plez, B., Thé, P. S., de Winter, D., Westerlund, B. E., & Steenman, H. C. 1994, A&AS, 105, 311
Garnett, D. R., & Shields, G. A. 1987, ApJ, 317, 82
Girardi, L., Bressan, A.,Chiosi, C., Bertelli, G., & Nasi, E. 1996, A&AS, 117, 113
Goerdt, A., & Kollatschny, W. 1998, A&A, 337, 699
Hill, J. K., et al. 1992, ApJ, 395, L37
Ho, L. C., Filippenko, A. V., & Sargent W. L. W. 1996, ApJ, 462, 183
Idiart, T. P., Thévenin, F., & de Freitas Pacheco, J. A. 1997, AJ, 113, 1066
Iglesias, C. A., Rogers, F. J., & Wilson, B. G. 1992, ApJ, 397, 717
Jablonka, P., Bica, E., Pelat, D., & Alloin, D. 1996, A&A, 307, 385
Kaufman, M., Bash, F. N., Crane, P. C., & Jacoby, G. H. 1996, AJ, 112, 1021
Kaufman, M., Bash, F. N., Hine, B., Rots, A. H., Elmegreene, D. M., & Hodge, P. 1989, ApJ, 345, 674
Kaufman, M., Bash, F. N., Kennicutt, R. C., Jr., & Hodge, P. 1987, ApJ, 319, 61
Kennicutt, R. C. 1998, ARA&A., 36, 189
Kong, X., & Cheng, F. Z. 1999, A&A, 351, 477
Kurucz, R. L. 1992, in IAU Symp. 149, The Stellar Population of Galaxies, ed. B. Barbuy & A. Renzini (Dordrecht: Kluwer), 255
Leitherer, C., et al. 1996, PASP, 108, 996
Leitherer, C., & Heckman, T. M. 1995, ApJS, 96, 9
Leitherer, C., et al. 1999, ApJS, 123, 3
Lejeune, Th., Cuisinier, F., & Buser, R. 1997, A&AS, 125, 229
———. 1998, A&AS, 130, 65
Mallik, S. V. 1994, A&AS, 103, 279
Mayya, Y. D. 1995, AJ, 109, 2503
———. 1997, ApJ, 482, L149
Mollà, M., Ferrini, F., & Diaz, A. I. 1997, ApJ, 475, 519
Origlia, L., Goldader, J. D., Leitherer, C., Schaerer, D., & Oliva, E. 1999, ApJ, 514, 96
Östlin, G., Bergvall, N., & Bönnback, J. 1998, A&A, 335, 85
Pagel, B. E. J., Edmunds, M. G., & Smith, G. 1980, MNRAS, 193, 219
Perelmuter, J.-M., Brodie, J. P., & Huchra, J. P. 1995, AJ, 110, 620
Salpeter, E. E. 1955, ApJ, 121, 161
Sawicki, M., & Yee, H. K. C. 1998, AJ, 115, 1329
Schaerer, D., & de Koter, A. 1997, A&A, 322, 598
Schaerer, D., & Vacca, W. D. 1998, ApJ, 497, 618
Schmitt, H. R., Bica, E., & Pastoriza, M. G. 1996, MNRAS, 278, 965
Searle, L., Sargent, W. L. W., & Bagnuolo, W. G. 1973, ApJ, 179, 427
Silva, L. 1995, Master's thesis, Univ. Padova
Stauffer, J. R., & Bothun, G. D. 1984, AJ, 89, 1702
Tantalo, R., Chiosi, C., Bressan, A., & Fagotto, F. 1996, A&A, 311, 361
Thuan, T. X. 1991, in Massive Stars in Starbursts, ed. C. Leitherer et al. (Cambridge: Cambridge Univ. Press), 183
Tinsley, B. M. 1972, A&A, 20, 383
Vazdekis, A., Peletier, R. F., Beckman, J. E., & Casuso, E. 1997, ApJS, 111, 203
Worthey, G., & Ottaviani, D. L. 1997, ApJS, 111, 377
Zheng, Z. Y., et al. 1999, AJ, 117, 2757
Zhou, X. 1991, A&A, 248, 367
Zombeck, M. V. 1990, Handbook of Space Astronomy and Astrophysics (2nd. ed; Cambrigde: Cambridge Univ. Press)